Controlling Morphology and Wettability of Intrinsically Superhydrophobic Copper-Based Surfaces by Electrodeposition

Raziyeh Akbari [1,2,3,*], Mohammad Reza Mohammadizadeh [1], Carlo Antonini [3], Frédéric Guittard [2] and Thierry Darmanin [2]

1   Supermaterials Research Laboratory (SRL), Department of Physics, University of Tehran, North Kargar Ave., Tehran P.O. Box 14395-547, Iran
2   NICE Lab, Université Côte d'Azur, Parc Valrose, 06108 Nice, France
3   Department of Materials Science, University of Milano-Bicocca, Via R. Cozzi 55, 20125 Milano, Italy
*   Correspondence: raziyeh.akbari@unimib.it

Abstract: Electrodeposition is an effective and scalable method to grow desired structures on solid surfaces, for example, to impart superhydrophobicity. Specifically, copper microcrystals can be grown using electrodeposition by controlling deposition parameters such as the electrolyte and its acidity, the bath temperature, and the potential modulation. The aim of the present work is the fabrication of superhydrophobic copper-based surfaces by electrodeposition, investigating both surface properties and assessing durability under conditions relevant to real applications. Accordingly, copper-based layers were fabricated on Au/Si(100) from $Cu(BF_4)_2$ precursor by electrodeposition, using cyclic voltammetry and square-pulse voltage approaches. By increasing the bath temperature from 22 °C to 60 °C, the growth of various structures, including micrometric polyhedral crystals and hierarchical structures, ranging from small grains to pine-needle-like dendrite leaves, has been demonstrated. Without any further physical and/or chemical modification, samples fabricated with square-pulse voltage at 60 °C are superhydrophobic, with a contact angle of 160° and a sliding angle of 15°. In addition, samples fabricated from fluoroborate precursor are carefully compared to those fabricated from sulphate precursor to compare chemical composition, surface morphology, wetting properties, and durability under UV exposure and hard abrasion. Results show that although electrodeposition from fluoroborate precursor can provide dendritic microstructures with good superhydrophobicity properties, surfaces possess lower durability and stability compared to those fabricated from the sulphate precursor. Hence, from an application point of view, fabrication of copper superhydrophobic surfaces from sulphate precursor is more recommended.

Keywords: wetting; electrodeposition; nanostructure; copper; durability

1. Introduction

In recent years, the use of water-repellent surfaces has increased in industrial applications due to their application as self-cleaning, antibacterial and anticorrosion surfaces, as well as drag reduction in marine applications [1–4]. Water repellence is achieved by minimizing the contact area between the surface and the water drop, and can be understood by studying the static contact angle θ_S [5]. As argued by Cassie and Baxter, surface hydrophobicity is correlated to the surface texture and to the material's intrinsic hydrophobicity [6–8], which is determined by the chemical composition. According to the Cassie-Baxter model, air pockets trapped inside the surface textures can prevent liquid from penetrating grooves, increasing water repellency and reducing drop–substrate adhesion. Specifically, complex hierarchical structures with micro- and nanometer features have been found to be ideal for stable superhydrophobicity [6,9,10]. To assess surface wetting properties in addition to static contact angle, θ_S, a study on the wetting hysteresis in quasi-static conditions is also crucial for investigating the wetting state of a solid surface. The wetting hysteresis (H)

is defined as the difference between the largest and lowest contact angles of the drop on the solid surface, i.e., the advancing (θ_{Adv}) and the receding (θ_{Rec}) contact angles, respectively (being $H = \theta_{Adv} - \theta_{Rec}$). In the definition of a superhydrophobic sample from an application view, the sliding angle (SA), which is defined as the minimum tilting angle of surface where the water drop easily slides on the surface, is also important. According to literatures [5,6,9,10], H and SA should ideally be lower than 10°.

Among the different surface-fabrication methods, electrodeposition is an effective and scalable method for the fabrication of textured surfaces with micrometric crystals of conductive materials, including metals, for example, copper for water-repellent surfaces [11,12] and cobalt–nickel alloy for anticorrosion application [13] and conductive polymers for porous structures [14]. Furthermore, electrodeposition is a cost-effective, scalable, and relatively fast method, which is already widely used in several industrial sectors for surface treatment and finishing. Indeed, electrodeposition can be used to control the surface roughness and morphology for the discovery and development of novel nanostructured materials with good mechanical properties [15,16]. Surface structures, spanning from 1D needles and fibres to 2D ribbons and sheets, and 3D hollow spheres, dendrites, and flower-like structures, can be used in many applications such as microelectronics, optoelectronics, lithium batteries, and biomedical applications [16–18]. In electrochemical deposition, also referred to as electrodeposition and electroplating, the electrolyte cell contains a working electrode (i.e., substrate), a counter electrode, and a reference electrode, immersed in an ionic conductor electrolyte solution (see schematic in Figure 1). Metal electrodeposition on the substrate occurs through the electrochemical reduction of ions from the electrolyte by applying an electric potential between the cathode (i.e., working electrode) and the anode (i.e., counter electrode). The potential drives the positive ions to migrate toward the extra electrons near the negatively charged cathode. During the deposition, metal ions are reduced and form a crystalline structure on the substate surface. The layer thickness is mainly determined by the electrodeposition conditions, including electrolyte chemical composition, bath temperature, deposition time, current, voltage, and modulation method [17,19–22]. Increasing the electrodeposition time in a highly reactive environment, for example, by increasing the number of deposition cycles in the cyclic voltammetry, or increasing the number of pulses in the pulse-voltage electrodeposition, results in a more intense and rapid deposition, which can increase the growth of more complex and vertical structures on the surface [17]. According to studies relating wettability to surface roughness [6,9,10,23], surface morphology, combined with the surface chemistry, has a significant influence on the wettability. Briefly, an increase in surface roughness enhances the surface properties, and thus can make a hydrophobic surface even more hydrophobic. Higher roughness can be achieved by increasing the deposition time, and eventually reaching superhydrophobicity.
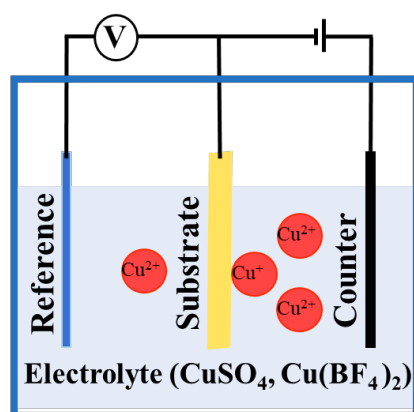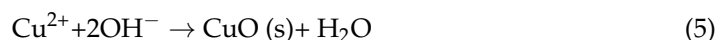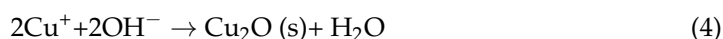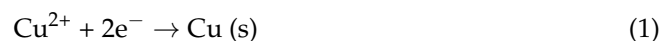

Figure 1. A schematic of an electrodeposition cell for depositing copper from an electrolyte containing copper sulphate or copper tetrafluoroborate solutions. A counter electrode repulses copper ions to the substrate. A reference electrode controls the reaction.

Since copper is widely used in several industrial networks, including water and electricity networks, solar energy and transportation [24–26], adding superhydrophobicity to the copper-based industrial surfaces will apply self-cleaning capability to these surfaces and increase the durability of the surfaces under wet conditions. To create copper-based layers using electrodeposition, various precursors are used in the industry, including sulphates, fluoroborates, acetates, alkyls and chlorides [17,27–30]. Previous studies have shown that the required potential for copper electrodeposition from the acid solution is less than that from alkaline solution, due to the higher conductivity and lower electrode polarization [17,30]. Hence, electrode polarization can be neglected for low current densities in acidic solutions, where the deposition rate is relatively higher. For the specific target of the fabrication of superhydrophobic copper-based surfaces, evidence is needed to identify which copper precursor provides better performances in controlling surface wetting properties. Among all, fluoroborate and sulphate precursors have the highest application potential for a variety of reasons: fluoroborate can lead to thicker layers; sulphate leads to homogeneously shaped layers and is abundant in the mineral residues. Thus, since the acidity of copper fluoroborate is higher than other acidic copper precursors such as sulphates, it does not require addition of acids to increase the electrochemical activity of the electrolyte [17]. By using copper fluoroborate solution dissolved in dodecylbenzene sulphonic acid sodium salt (DBSA) and poly(vinylpyrrolidone) (PVP), which act as ion stabilizer in the electrolyte solution, Ko et al. [31] reported the fabrication of various copper architectures such as pyramids, cubes, and multipods. Tetrahedral pyramids were grown in the ratio of 1:3 from copper and DBSA solution [31]. By decreasing the ratio to 1:2, the created crystals on the surface converted to free-standing cubes [32], whereas multipods were observed for copper solution in PVP [33]. PVP acts as a capping surfactant reagent, which is adsorbed differently on various crystal surfaces and leads to a competitive growth between different copper crystal facets, and results in shape variation of the final crystal shape. According to the literature [31,34–37], some of possible reactions in an aqueous solution of copper during the electrodeposition are as follows:

$$Cu^{2+} + 2e^- \rightarrow Cu\ (s) \tag{1}$$

$$Cu^{2+} + e^- \rightarrow Cu^+ \tag{2}$$

$$Cu^+ + e^- \rightarrow Cu\ (s) \tag{3}$$

$$2Cu^+ + 2OH^- \rightarrow Cu_2O\ (s) + H_2O \tag{4}$$

$$Cu^{2+} + 2OH^- \rightarrow CuO\ (s) + H_2O \tag{5}$$

The application of a negative voltage between the counter electrode and the substrate can convert Cu^{2+} ions to Cu deposits on the substrate (Equation (1)) if the absolute value of voltages is higher than the reduction potential. For an absolute value of voltages lower than the reduction potential, there is also a possibility of a two-step reduction in the Cu^{2+} ions to Cu: firstly, Cu^{2+} converts to Cu^+, and then Cu^+ absorbs an electron and reduces to Cu deposits on the substrate, following Equations (2) and (3), respectively. A third reduction mechanism is based on partial reaction of copper ions with hydroxide ions in the electrolyte following Equations (4) and (5). These conditions can lead to an increase in the copper oxide content of the deposited layer in the higher temperatures. In addition, the reactivity and wetting of the as-prepared copper layers from aqueous solution can also increase the amount of adsorbed oxygen on the layer surface, which can be higher in highly rough-structured layers [28,29,38].

The present study first conducts a systematic investigation of the electrodeposition of fluoroborate precursors, using both cyclic voltammetry and square-pulse voltage in an aqueous solution. All samples from fluoroborate precursors (referred to as fluoroborate samples or fluoroborate surfaces for brevity) are characterized by goniometry, profilometry, scanning electron microscopy, and X-ray diffraction, to correlate electrodeposition parameters to surface morphology and wettability. The aim of the present work is the fabrication

of superhydrophobic copper-based samples and investigating its surface properties and durability for real applications. Thus, following our previous studies on samples from copper sulphate precursor [27–29,38] (referred to as sulphate samples or sulphate surfaces for brevity), a comparison between the use of the two precursors is presented here to provide an overall assessment of surface morphology, chemistry, hydrophobicity, and durability.

2. Materials and Methods

2.1. Electrodeposition Conditions

An aqueous solution from 0.1 M copper (tetra-)fluoroborate precursor (Sigma Aldrich, St. Louis, MI, USA) with pH = 3.15 was prepared to deposit copper and copper oxides on Au/Si(100) substrates using both cyclic voltammetry and square-pulse voltage at bath temperatures of 22, 45, and 60 °C (see [27,29,38]). The electrochemical system included an Autolab potentiostat of Metrohm with three connected electrodes: (i) a 150 nm Au on Si(100) wafer as working electrode, (ii) a carbon rod as counter electrode, and (iii) a saturated calomel (SCE) as reference electrode. In the squared-pulse voltage deposition (referred to as "pulse" for convenience), each deposition cycle consisted of 10 s deposition at a fixed working voltage of $E_W = -0.3$ V and subsequently 2 s relaxing at 0 V, following our previous studies [27–29,38]. Deposition cycles were repeated 8 or 12 times at three bath temperatures. In cyclic voltammetry deposition (referred to "CV"), cycles were repeated 3 or 5 times at three bath temperatures, with voltage in the range $[-0.3, 0]$ V and a scan rate of 20 mV/s. The prepared samples were washed in distilled water and dried for one week in a sealed glass box in ambient conditions before characterization.

2.2. Surface Characterization

A Wyko NT1100 optical microscope (Bruker) with high-magnification vertical scanning interferometry (VSI), a field of view 0.5X, objective 50X, and scan size 239×182 μm was used to measure the average surface roughness ($R_{a,O}$). $R_{a,O}$ is measured noncontact using optical interferences. Since there is a divergence between roughness numbers measured by stylus and optical methods (see [39–41]), specially in highly rough and dendrite surfaces, the roughness measured in this article is named as $R_{a,O}$ to indicate the measurement method. Surface morphology was imaged by scanning electron microscopy (SEM) machines including 6700F JEOL and Vega TS5136 XM Tescan microscopes. A Philips XRD X'pert MPD diffractometer (Cu Kα radiation, 1.54 Å) with a step size of 0.02° and count time of 1 s per step in 2θ, ranging from 10° to 80°, was used to provide X-ray diffraction (XRD) patterns of the samples. The wetting properties of the samples were measured using a DSA30 goniometer (Krüss) as well as an in-home contact angle measurement set-up consisting of a high-speed camera (PHOTRON-NOVA FASTCAM S6, 1:1 Tokina AT-X M100 PRO D lens, 20 μm pixel size) with 2 to 7 μL water drops ($\gamma LV = 72.8$ mN/m), repeating the measurement in at least three different positions for each sample. The drop size for sliding-angle (SA) measurements was 5 μL. The contact angle images and videos were analyzed using Dropen, an open-source in-house-developed software [42]. A low-intensity UV oven (SHAREBOT UCB), 405 nm wavelength, 120 W power, with ~20 cm lamp–sample distance, was used for surface cleaning in periods of 5 to 150 minutes. Abrasion tests were performed using a dedicated test setup consisting of sandpaper, a weight, and a ruler. As shown in the side view in Figure 2 the back side of the sample was attached to a glass slide using an adhesive tape and placed on P1500 SiC sandpaper. A 100 g weight was placed on the glass to increase the contact and pressure between the sample and the sandpaper. The test was performed by pulling the sample on the sandpaper along different distances, up to 30 cm. After every 3 cm of abrasion, the static and quasi-static (i.e., advancing and receding) contact angles were measured.
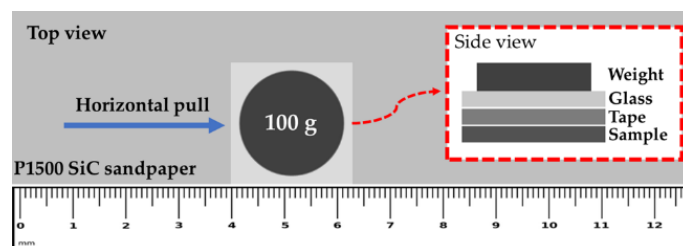
Figure 2. A schematic of the abrasion test setup used in this paper. It consisted of sandpaper, weight, and ruler. As shown in the side view, the sample was attached to a glass slide from its backside and placed on the sandpaper. The test was performed by pulling the sample on the sandpaper along different distances, as a 100 g weight was placed on the sample. After every 3 cm, the wetting state of the sample was examined.

3. Results

The results of the electrodeposition of copper from 0.1 M copper (tetra-)fluoroborate at 22, 45, and 60 °C using square potential pulse and cyclic voltammetry methods are presented, including XRD spectrum, contact angle values, roughness, and SEM images to visualize surface morphology.

3.1. Square Pulse

Chemistry and morphology of the prepared samples using the square-pulse method have been investigated to find the influence of the surface characteristics on the hydrophobicity. The XRD measurements show that Cu and Cu_2O facets in (111) direction are the only components in the deposited layer (see Figure 3). According to the results, the amount of copper is decreased by increasing the bath temperature while the amount of copper oxide is increasing, whereas at 60 °C, copper and copper oxide have similar intensities. A similar behaviour is observed in the sulphate samples [38]. Previous studies [23,27,38] have shown that due to high reactivity of copper structures especially in noncrystalline, highly rough, and fine-grained wet surfaces, it is expected that highly rough copper surfaces partially react with air under the ambient conditions after deposition while they are still wet and reactive. Hence, a slight change in the surface chemical composition towards more oxidation is considerable in this condition.
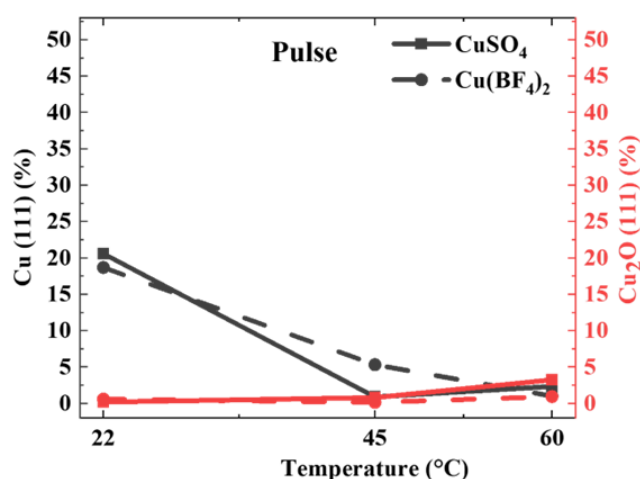

Figure 3. A comparison between the main Cu and Cu_2O peaks (both in (111) direction) in XRD spectrum of the prepared samples by pulse method using sulphate and fluoroborate precursors. The relative intensities are reported in % in comparison to the largest XRD peak of the substrate (i.e., Au (111)).

Figure 4a,b show that with every 15 °C increase in the deposition temperature, surface roughness increases by an order of magnitude. Hence, the roughness at 22, 45, and 60 °C

is around 20 nm, 200 nm, and 1 µm, respectively. In addition, wetting measurements (see Figure 4a,b) show that θ_S increases by increasing the surface roughness as well as the number of pulses. In addition, the highest θ_S is observed in samples of 60 °C, reaching 156° in 8 pulses, and increasing to 160° in 12 pulses with five times larger roughness. This large roughness and superhydrophobic behaviour indicate the formation of a complex hierarchical structure, which causes the improvement of the surface water repellency, according to the Cassie–Baxter equation [6]. This is confirmed by SEM images, Figure 5.
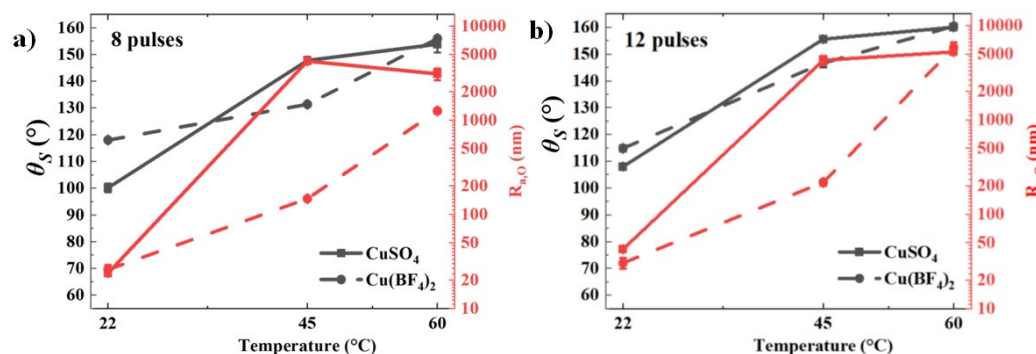

Figure 4. A comparison in contact angle and roughness of prepared samples from sulphate and fluoroborate solutions using pulse method in (**a**) 8 and (**b**) 12 numbers of deposition pulses. θ_S of the uncoated substrate is 85°.
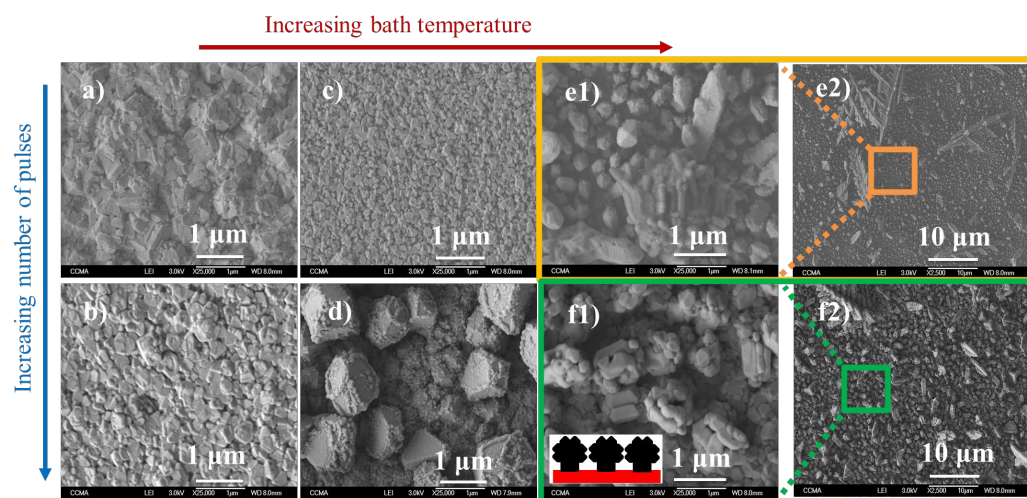

Figure 5. SEM images of the samples prepared from fluoroborate precursor using pulse method. (**a**) 22 °C, 8 pulses, nominal grain size (D_g) ≈ 300–500 nm; (**b**) 22 °C, 12 pulses, D_g ≈ 200–400 nm; (**c**) 45 °C, 8 pulses, D_g ≈ 60–200 nm; (**d**) 45 °C, 12 pulses, D_g ≈ 1–1.3 µm; (**e1**) 60 °C, 8 pulses, D_g ≈ 500 nm–1.2 µm; (**e2**) a larger view of e1 with fractal trees of around 15 µm; (**f1**) 60 °C, 12 pulses, D_g ≈ 300–600 nm, presented in a larger view in (**f2**) with fractal trees with different lengths from 3 to 20 µm. A schematic pattern of hierarchical structures is shown in f1.

According to Figure 5a, the structure formed at 22 °C is an accumulation of crystallites, a few hundred nm in diameter, with flat facets in various tetrahedron shapes. The size and out-of-plane growth of the structures are decreased by increasing the number of pulses (Figure 5b). In addition, although most of the crystal facets are tetrahedrons in 8 pulses, they are more likely to be broken triangles (i.e., hexahedron) in 12 pulses. Thus, the ability to follow the growth regime is weakened by increasing the number of deposited layers. At 45 °C, initially, in 8 pulses, a similar structure to 22 °C is grown (Figure 5c). By increasing the deposition pulses (Figure 5d), the size of crystals is increased significantly contradictory to the deposition in ambient temperature. This has led to the formation of micrometric octahedral crystals with deep valleys in between and increases θ_S to 147°. At

60 °C, changes in the surface structure are more prominent where different dendrite and hierarchical structures are formed on the sample (see Figure 5e1,e2), which is a result of instabilities in the solvent at this temperature due to approaching the boiling temperature of the solution. According to our experiments, the deposition rate in fluoroborate solution is considerably low in bath temperatures higher than 60 °C. The formed structures include (1) standing fractal leaves in 15 μm length, longer than our previous samples prepared by copper sulphate precursor [28,38]; (2) Step-like hierarchical structures formed upon a larger crystal with an average diameter of 1 μm; (3) 3D octahedral pyramids with diameters ranging from 300 to 500 nm, similar to [29]. The formation of this complex structure leads to a sharp increase in surface roughness, resulting in an increase in θ_S to 155° for 8 pulses. However, the drop remains stuck on the surface and the sample is not superhydrophobic, an intermediate state between Wenzel and Cassie–Baxter [9], possibly due to the heterogeneity of surface roughness. By increasing the deposition to 12 pulses, partially ordered pine-like structures with lengths of 3 to 20 μm are observed on the surface (see Figure 5f2). Therefore, increasing the number of sharp vertical needles and more ordering and hierarchy in the small crystals formed between large structures, as well as critically larger roughness, lead to an increase in θ_S to 160°, where the water drop rolls down from the surface by tilting the surface to 15° for a 5 μL drop.

3.2. Cyclic Voltammetry

To study the changes in the surface hydrophobicity by electrodepositing copper from the fluoroborate solution, samples prepared by cyclic voltammetry are investigated through the chemical and physical characteristics. According to Figure 6, the cyclic voltammetry samples are covered by Cu(111). The amount of Cu_2O in the samples is negligible. According to the last observations [27–29,38], the very high intensity for Cu at 60 °C in respect to the lower temperature could be a result of the formation of a significantly thicker layer.
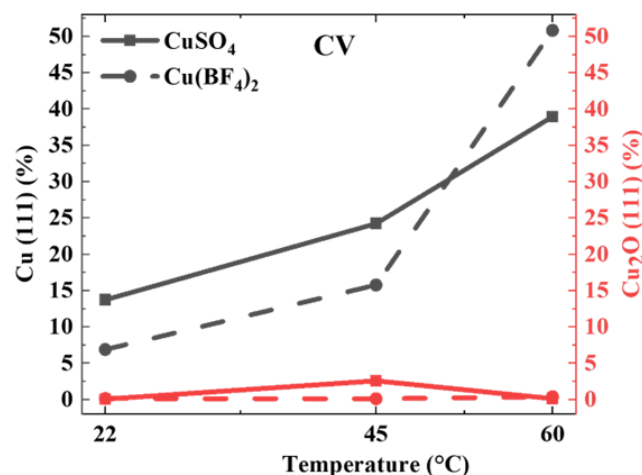

Figure 6. A comparison between the main Cu and Cu_2O peaks (both in (111) direction) in XRD spectrum of the prepared samples by CV method using sulphate and fluoroborate precursors. The relative intensities are reported in % in comparison to the largest XRD peak of the substrate (i.e., Au (111)).

Figure 7a,b show that the roughness is increased significantly by increasing the bath temperature and the number of deposition cycles. In '60 °C, 5 cycles', the roughness reaches the maximum of ~2 μm due to creation of complex hierarchical structures. According to the θ_S results, the hydrophobicity in the samples follows the roughness changes and increases by increasing the bath temperature and the number of deposition cycles. Hence, the wetting in CV samples is in the Wenzel state and reaches 137° at maximum roughness.
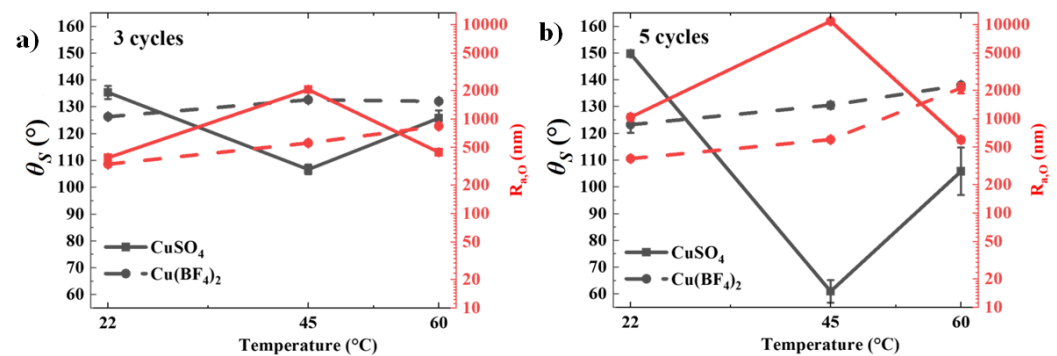
Figure 7. A comparison in contact angle and roughness of prepared samples from sulphate and fluoroborate solutions using CV method in (**a**) 3 and (**b**) 5 numbers of deposition cycles. θ_S of the uncoated substrate is 85°.

The surface of the '22 °C, 3 cycles' sample shown in Figure 8a consists of submicron octahedral crystallites with flat facets formed between smaller flat crystals, 1μm in diameter. The size of the small structures formed between large structures is increased by further deposition at the same bath temperature, i.e., '22 °C, 5 cycles', whereas the number and the size of the upper flat crystals are reduced (see Figure 8b). Thus, the growth of large structures and their out-of-plane growth were intensively increased by increasing the number of deposition cycles. Crystallites twice the size are grown at '45 °C, 3 cycles' compared to the samples fabricated in 22 °C (Figure 8c) while the shape of the crystallites is almost similar in these two bath temperatures. The size of structures and their out-of-plane growth are increased significantly by increasing the number of deposition cycles in 45 °C, whereas larger crystals ~5 μm in diameter and deeper and wider valleys are formed on the surfaces fabricated in 5 cycles (Figure 8d). The growth regime of the surface structure, i.e., the growth of micrometric surface crystallites with flat facets, as well as an increase in the size and the out-of-plane growth of crystallites by increasing the bath temperature and the number of deposition cycles, are followed at '60 °C, 3 cycles' (Figure 8e1,e2), whereas the size of the crystals is ~4 times larger than '45 °C, 3 cycles'. Thus, increasing the bath temperature prepares good conditions for the growth of large microcrystals and increases the crystallinity of the sample, in agreement with the previous observations [43–46]. Moreover, due to the increase in the mobility of copper ions towards the substrate at 60 °C, a temperature close to the boiling point of the electrolyte solution, some vertical aggregated structures are also observed in a larger view to the surface of '60 °C, 3 cycles', Figure 8e2. By increasing the number of deposition cycles at 60 °C, the vertical growth was expanded and became the prominent surface growth regime. Thus, vertical leaves with a length of ~3–10 μm are effectively grown in '60 °C, 5 cycles' (Figure 8f1,f2). This dendritic growth is due to the increase in the formation of air bubbles at 60 °C, close to the boiling point of the solution, and subsequent instability in the electrochemical conditions of the deposition. The surface between the leaves is covered with an aggregation of broken flat crystallites (Figure 8f1), which is smaller than the pulse samples (see Figure 5f1). The shape of the surface structures in '60 °C, 5 cycles', including the dendrite vertical leaves with sharp tips and the broken pyramids between the leaves, is substituted into Figure 8f2.
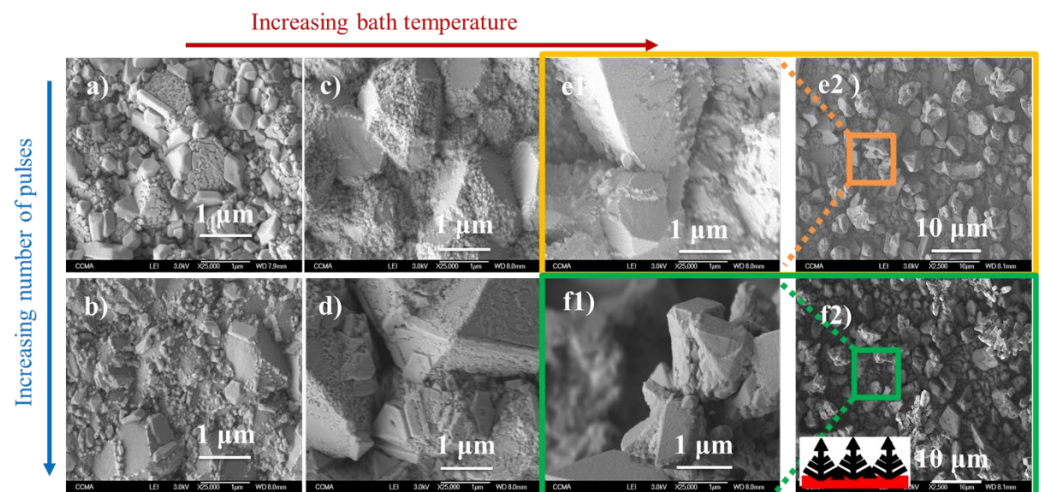
Figure 8. SEM images of the samples prepared from fluoroborate precursor using CV method. (**a**) 22 °C, 3 cycles, D_g: 200–700 nm on 1–1.2 µm grains; (**b**) 22 °C, 5 cycles, $D_g \approx$ 1–1.6 µm; (**c**) 45 °C, 3 cycles, $D_g \approx$ 1.5–2.5 µm; (**d**) 45 °C, 5 cycles, $D_g \approx$ 4–5 µm; (**e1**) 60 °C, 3 cycles, $D_g \approx$ 3–5.5 µm; (**e2**) a larger view of (**e1**); (**f1**) 60 °C, 5 cycles, with average tip sizes of 0.3–2 µm, in a larger view in (**f2**) with fractal trees length >10 µm, and a schematic pattern of the grown structure on the surface.

3.3. Wetting Durability

3.3.1. Under UV Exposure

To investigate the durability of wetting on the prepared copper thin layers, three samples with different surface structures, including micrometric crystals, dendrites, and hierarchical structures, were chosen (details in Figure 9).
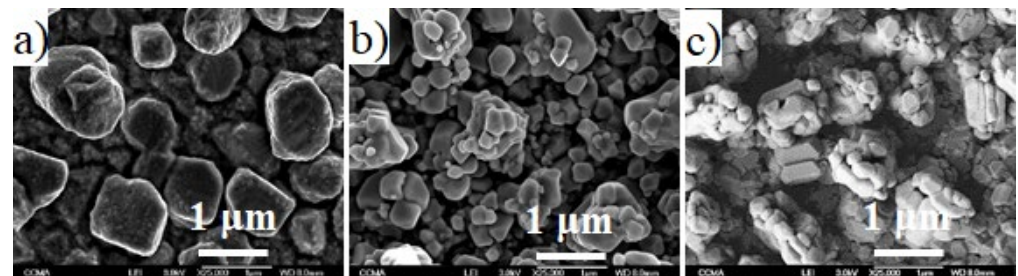

Figure 9. SEM image of the samples chosen for the comparison between samples prepared by sulphate and fluoroborate precursors: (**a**) 'CuSO$_4$, 15 °C, 7 cycles', Cu(111) = 0.93%, Cu$_2$O (111) = 0.48%, $R_{a,O}$ = 806 ± 41 nm, crystal size < 1 µm, θ_S = 142°; (**b**) 'CuSO$_4$, 60 °C, 12 pulses', Cu(111) = 2.33%, Cu$_2$O (111) = 3.23%, $R_{a,O}$ = 5260 ± 387 nm, crystal size < 1 µm, θ_S = 160°, SA = 22°; (**c**) Cu(BF$_4$)$_2$, 60 °C, 12 pulses, Cu(111) = 0.92%, Cu$_2$O in (111) = 0.99%, $R_{a,O}$ = 5877 ± 747 nm; crystal size < 0.6 µm, θ_S = 160°, SA = 15°.

As discussed in our previous papers [23,27–29,38], hydrophobicity of the copper samples increases by aging in a sealed glass bottle. This change in contact angle could be a result of the contamination of sample with hydrocarbons in air, which is higher in the more-structured surfaces, i.e., dendrite and hierarchical surfaces, while the contact angle of as-prepared 'CuSO$_4$, 15 °C, 7 cycles', 'CuSO$_4$, 60 °C, 12 pulses', and 'Cu(BF$_4$)$_2$, 60 °C, 12 pulses' samples are 142°, 160°, and 160°, respectively (see Figure 9). Among these three samples, only 'CuSO$_4$, 60 °C, 12 pulses' shows good superhydrophobicity, and the water drop bounces on it (see Figure 10). Accordingly, during 200 ms after dropping a water drop, 1.36 mm in diameter, on the surface from 2.28 mm distance, the drop bounces six times before depositing on the substrate.
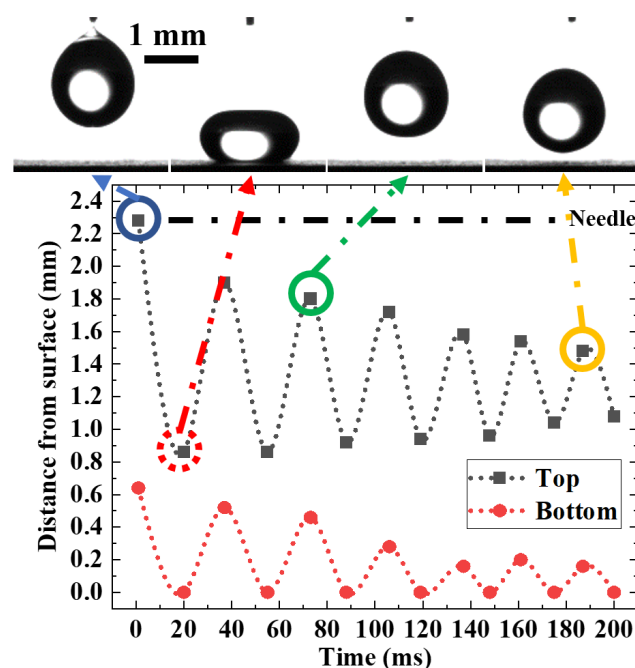
Figure 10. Six cycles of bounding, rebounding, bouncing of water drop on 'CuSO$_4$, 60 °C, 12 pulses' surface. Needle distance from the surface = 2.28 mm. Drop diameter = 1.36 mm.

According to the previous studies [47–49], superhydrophobicity in some metals is a result of the hydrocarbon adsorption on the surface from air and is not an intrinsic property. Hence, it is expected that UV irradiation cleans the surface from contaminations [50,51] and reduces its hydrophobicity. To study this effect, the wettability evolution under UV exposure is tracked up to 150 minutes and the results are shown in Figure 11. The highly hierarchical 'CuSO$_4$, 60 °C, 12 pulses' sample is still superhydrophobic even after 150 minutes: the contact angle is reduced from 160° to 145° during the initial 30 minutes of UV exposure and subsequently remains constant. As such, the surface is intrinsically superhydrophobic, and hydrocarbon adsorption does not play any role on the observed wetting behaviour of such surfaces. Differently, on 'CuSO$_4$, 15 °C, 7 cycles' and 'Cu(BF$_4$)$_2$, 60 °C, 12 pulses' the contact angle is reduced to ~125° in the first 70 minutes of UV exposure, and then remains constant. Thus, the samples are still hydrophobic, but not superhydrophobic anymore, suggesting that on these two surfaces hydrocarbon adsorption partially plays a role in conferring the initially observed superhydrophobicity. In order to study the wetting hysteresis in the exposed samples, advancing and receding contact angles of these samples were also measured.

According to Figure 12, the contact angle in 'CuSO$_4$, 15 °C, 7 cycles', 'CuSO$_4$, 60 °C, 12 pulses', and 'Cu(BF$_4$)$_2$, 60 °C, 12 pulses' is increased from 123°, 142°, and 128° just after the irradiation to 128°, 160°, and 142° after one week rest in the sealed glass bottle, respectively. Meanwhile, two less hydrophobic samples show a large hysteresis with a very low receding contact angle (i.e., $20° < \theta_{Rec} < 30°$), while 'CuSO$_4$, 60 °C, 12 pulses' is highly nonwettable with 6° wetting hysteresis. As a result of this study, the 'CuSO$_4$, 60 °C, 12 pulses' sample with a highly textured hierarchical surface is intrinsically superhydrophobic and is not highly affected by environmental contamination and UV irradiation. However, in the two less-structured surfaces, superhydrophobicity is less stable after cleaning with UV light, and superhydrophobicity in these two samples could be a result of the surface contamination.
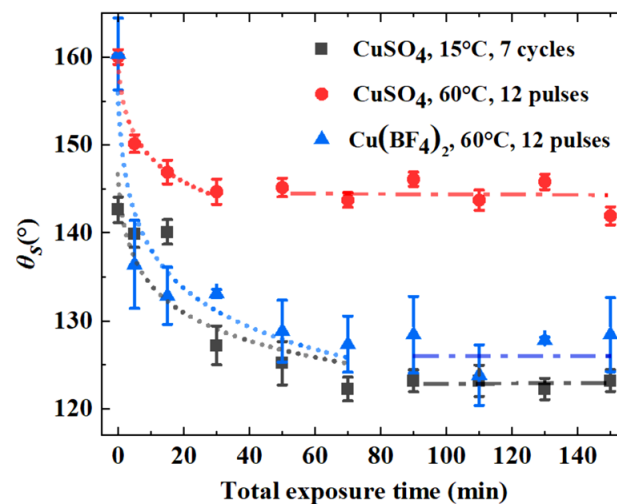
Figure 11. Changes in contact angle after UV exposure with 150 W power at 20 cm distance. Dotted lines show a power fitting to the data in reduction regime. Dash-dot lines represent the almost constant contact angles after reduction regime.
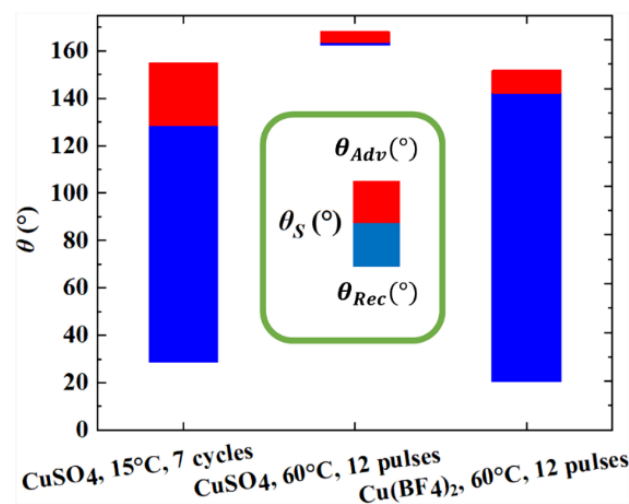

Figure 12. Static, advancing, and receding contact angles of the selected samples two days after UV exposure.

3.3.2. Abrasion Tests

In order to evaluate the stability of wetting in the selected highly rough fluoroborate and sulphate samples (i.e., 'Cu(BF$_4$)$_2$, 60 °C, 12 pulses' and 'CuSO$_4$, 60 °C, 12 pulses') under abrasion with sandpaper, the following test based on the ASTM D4060 standard [52] was performed.

As discussed in the supplementary of [38], the size of surface grooves after abrasion depends on the hardness of the surface structure, which influences the wetting stability of the sample in real harsh environments such as car or aircraft outside surfaces. According to Figure 13, after 30 cm hard abrasion, deep grooves with 6 and 18 μm width on average are created on the sulphate and fluoroborate samples, respectively. In a real application, the static contact angle and wetting hysteresis (i.e., $H = \theta_{Adv} - \theta_{Rec}$) are important.
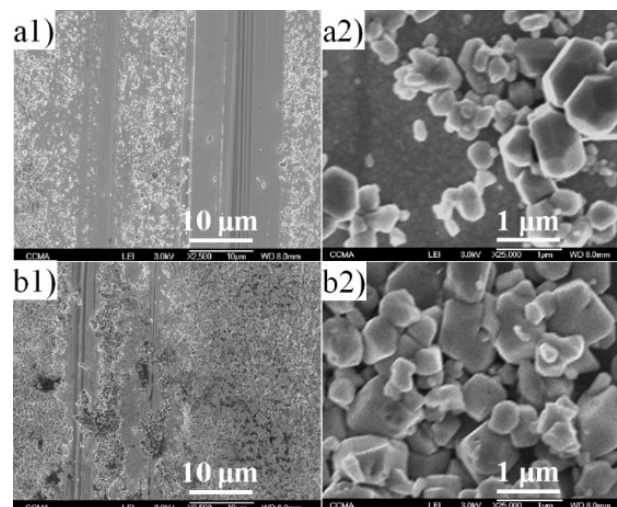
Figure 13. SEM images of (**a1,a2**) 'Cu(BF$_4$)$_2$, 60 °C, 12 pulses'; and (**b1,b2**) 'CuSO$_4$, 60 °C, 12 pulses', after 10-cycle abrasion with P1500 SiC sandpaper.

As shown in Figure 14, while the wetting state in the sulphate sample after a hard abrasion for 10 cycles is changed by 20° with maximum 6° hysteresis and is still highly hydrophobic, the fluoroborate sample faces a reduction in contact angles of ~40°. Moreover, while the sulphate samples remain constant in abrasion lengths larger than 12 cm, the wettability of the fluoroborate sample decreases even after 30 cm abrasion. Therefore, although the metal oxide surface will be destroyed after a hard abrasion with SiC sandpaper on the sulphate sample, the surface is still hydrophobic and shows a good wear resistance and is still reliable for practical applications under harsh environmental conditions.
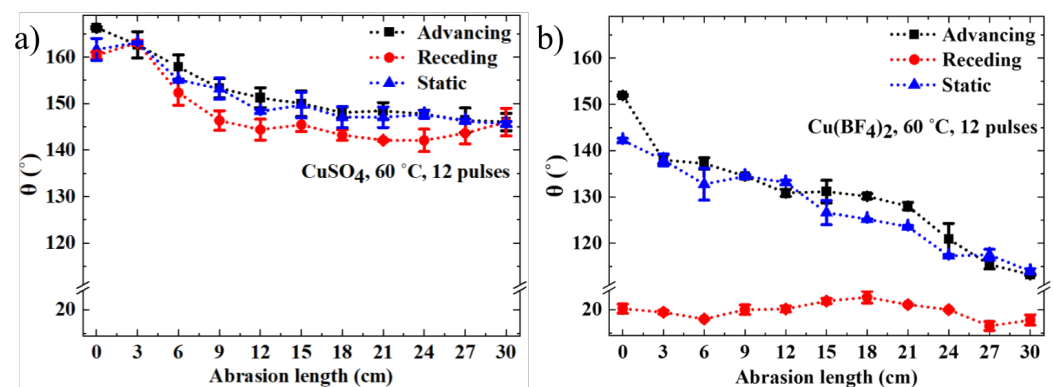

Figure 14. Changes in the advancing, receding, and static contact angles of (**a**) 'CuSO$_4$, 60 °C, 12 pulses' and (**b**) 'Cu(BF$_4$)$_2$, 60 °C, 12 pulses' samples under a hard abrasion for 10 cycles.

3.4. A Comparison between the Sulphate and Fluoroborate Samples

According to the present and our previously published works [29,38] on the fabrication of superhydrophobic copper surfaces using the electrodeposition method, the surface structures formed in the electrodeposition of copper using sulphate and fluoroborate precursors include (a) 3D crystals with flat facets in triangular, square and hexahedron shapes; (b) 100 nm balls grown on a coverage of micrometric octahedral crystals; (c) 10 to 20 μm fractal leaves with complex shapes and multiple branches and trunks, particularly with sharp octahedral crystals at the branch tips; and (d) a hierarchical micrometric combination of the previous structures. Accordingly, a comparison between the copper fluoroborate and sulphate prepared samples can be conducted as follows. Our experiments show that the maximum applicable bath temperature for aqueous solution is 65 and 90 °C [29] in fluoroborate and sulphate, respectively. Through the roughness curves, Figures 4 and 7, it

could be concluded that the deposition rate of sulphate is higher than fluoroborate. A more careful study on both the lateral and vertical surface morphology is needed to approve this hypothesis. In the sense of chemical composition, a partial creation of the oxide grains after deposition under the air exposure due to higher porosity of the samples prepared in higher temperatures results a near decrease in the height of Cu(111) and increase in $Cu_2O(111)$ by increasing the bath temperature in the samples prepared by the square-pulse method from sulphate and fluoroborate precursors, while the amount of copper oxide is still significantly lower than copper (Figure 3). Contrary to pulse samples, in cyclic voltammetry samples the XRD patterns (Figure 6) show the stability of copper in the system and the height of the Cu(111) peak is effectively increased by increasing the bath temperature, which could be a sign of the rapid increase in the layer thickness. Surface morphology and wetting studies show that increasing the bath temperature in the pulse voltage method increases the roughness and porosity rapidly by growing hierarchical and dendrite leaves on the surface of the copper samples, whereas the surface reaches the optimum structure and shows superhydrophobicity with $\theta_S > 150°$ and SA < 25° in an optical roughness (i.e., $R_{a,O}$) of around 5000 nm at 60 °C in both the sulphate and fluoroborate precursors (see Figure 4a,b). Nonetheless, the rapid increase in the roughness happens at 45 and 60 °C in sulphate fluoroborate samples, respectively. SEM images (Figure 7 of [38] and Figure 5) confirm the increase in the surface complexity in samples prepared from the both precursors, while the growth of a fully hierarchical surface structure with sharp tips and very low solid fraction in contact with the water drop in samples prepared at 60 °C provides enough qualifications for the creation of Cassie–Baxter conditions on the surface. The evolution rate of the surface structure in fluoroborate samples by increasing the bath temperature is lower than the sulphate samples. While the roughness and the contact angle in the fluoroborate samples prepared by cyclic voltammetry method has a similar trend, in samples prepared from sulphate precursor, the sample with higher roughness shows a lower contact angle (Figure 7) due to the powdery nature of the sample, and the water spreads over powder particles on the surface.

Durability tests of the samples on UV exposure and hard abrasion show the instability of the wetting state in the fluoroborate sample and its changes in the various environmental conditions, including UV light exposure and hard abrasion (Figures 11 and 14). Thus, the wetting state of the sulphate and fluoroborate samples is different, although these samples show a similar static contact angle and sliding angle in the as-prepared samples. This result emphasizes the importance of quasi-static wetting studies and systematic durability investigations in the superhydrophobic samples, which are going to be more noticed by scientists [53].

4. Conclusions

The present paper is an experimental study on the fabrication of robust superhydrophobic surfaces from copper-based precursors using electrodeposition. Specifically, both square-pulse voltage and cyclic voltammetry methods from copper fluoroborate precursor at different bath temperatures have been used. It has been observed that Cu and Cu_2O content on the deposited layer was affected by both the deposition temperature and the applied method. The increase in the bath temperature increased the roughness and water contact angle on the surface. Superhydrophobicity, with a contact angle of 160° and a sliding angle of 15°, was observed in the most structured surface fabricated by using pulse electrodeposition at 60 °C with 12 pulses: such sample has a hierarchical structure, including fractal leaves and submicron crystals. This sample was compared with a superhydrophobic sample fabricated from copper sulphate precursor, at the same deposition conditions, to investigate their durability under UV exposure and hard abrasion. It has been observed that on fluoroborate samples superhydrophobicity is not sustained, suggesting that hydrocarbon spontaneous adsorption from the atmosphere (which is removed by UV exposure) partially plays a role in conferring the initially observed superhydrophobicity. Differently, surfaces from sulphate precursor can sustain both UV exposure and hard abra-

sion, suggesting that they are intrinsically superhydrophobic, with no effect of hydrocarbon adsorption, and they can thus be more robust for industrial applications.

Institutional Review Board Statement: Not applicable.

Informed Consent Statement: Not applicable.

Data Availability Statement: Data is contained within the article.

Conflicts of Interest: The authors declare no conflict of interest.

References

1. Liu, J.; Huang, X.; Li, Y.; Li, Z.; Chi, Q.; Li, G. Formation of Hierarchical CuO Microcabbages as Stable Bionic Superhydrophobic Materials via a Room-Temperature Solution-Immersion Process. *Solid State Sci.* **2008**, *10*, 1568–1576. [CrossRef]
2. Zhang, P.; Lv, F.Y. A Review of the Recent Advances in Superhydrophobic Surfaces and the Emerging Energy-Related Applications. *Energy* **2015**, *82*, 1068–1087. [CrossRef]
3. Guittard, F.; Darmanin, T. *Bioinspired Superhydrophobic Surfaces: Advances and Applications with Metallic and Inorganic Materials*; Pan Stanford Publishing Pte Ltd, Ed.; Jenny Stanford Publishing: Stanford, CA, USA, 2017; ISBN 9781351859592.
4. Yifan Si, Z.G. Superhydrophobic Nanocoatings: From Materials to Fabrications and to Applications. *Nanoscale* **2015**, *7*, 5922–5946. [CrossRef]
5. Darmanin, T.; Guittard, F. Recent Advances in the Potential Applications of Bioinspired Superhydrophobic Materials. *J. Mater. Chem. A* **2014**, *2*, 16319–16359. [CrossRef]
6. Cassie, A.B.D.; Baxter, S. Wettability of Porous Surfaces. *Trans. Faraday Soc.* **1944**, *40*, 546–551. [CrossRef]
7. Khaskhoussi, A.; Risitano, G.; Calabrese, L.; D'andrea, D. Investigation of the Wettability Properties of Different Textured Lead/Lead-Free Bronze Coatings. *Lubricants* **2022**, *10*, 82. [CrossRef]
8. Volpe, A.; Covella, S.; Gaudiuso, C.; Ancona, A. Improving the Laser Texture Strategy to Get Superhydrophobic Aluminum Alloy Surfaces. *Coatings* **2021**, *11*, 369. [CrossRef]
9. Marmur, A. Hydro- Hygro- Oleo- Omni-Phobic? Terminology of Wettability Classification. *Soft Matter* **2012**, *8*, 6867–6870. [CrossRef]
10. Wenzel, R.N. Resistance of Solid Surfaces to Wetting by Water. *Ind. Eng. Chem.* **1936**, *28*, 988–994. [CrossRef]
11. Mumm, F.; Van Helvoort, A.T.J.; Sikorski, P. Easy Route to Superhydrophobic Copper-Based Wire-Guided Droplet Microfluidic Systems. *ACS Nano* **2009**, *3*, 2647–2652. [CrossRef]
12. Shirtcliffe, N.J.; McHale, G.; Newton, M.I.; Perry, C.C. Wetting and Wetting Transitions on Copper-Based Super-Hydrophobic Surfaces. *Langmuir* **2005**, *21*, 937–943. [CrossRef] [PubMed]
13. Wang, S.; Xue, Y.; Xue, Y.; Lv, C.; Jin, Y. Long-Term Durability of Robust Super-Hydrophobic Co–Ni-Based Coatings Produced by Electrochemical Deposition. *Coatings* **2022**, *12*, 222. [CrossRef]
14. Ramos Chagas, G.; Akbari, R.; Godeau, G.; Mohammadizadeh, M.; Guittard, F.; Darmanin, T. Electrodeposited Poly(Thieno[3,2-b]Thiophene) Films for the Templateless Formation of Porous Structures by Galvanostatic and Pulse Deposition. *Chempluschem* **2017**, *82*, 1351–1358. [CrossRef] [PubMed]
15. Darmanin, T.; De Givenchy, E.T.; Amigoni, S.; Guittard, F. Superhydrophobic Surfaces by Electrochemical Processes. *Adv. Mater.* **2013**, *25*, 1378–1394. [CrossRef]
16. Al-Bat'hi, S.A.M. Electrodeposition of Nanostructure Materials. In *Electroplating of Nanostructures*; Aliofkhazraei, M., Ed.; IntechOpen: London, UK, 2015; pp. 3–26.
17. Nasirpouri, F. *Electrodeposition of Nanostructured Materials*; Car, R., Ertl, G., Freund, H.J., Lüth, H., Rocca, M.A., Eds.; Springer: Cham, Switzerland, 2017; ISBN 9783319449197.
18. Gurrappa, I.; Binder, L. Electrodeposition of Nanostructured Coatings and Their Characterization—A Review. *Sci. Technol. Adv. Mater.* **2008**, *9*. [CrossRef]

19. Barnes, S.C.; Storey, G.G.; Pick, H.J. The Structure of Electrodeposited Copper-III. The Effect of Current Density and Temperature on Growth Habit. *Electrochim. Acta* **1960**, *2*, 195–204. [CrossRef]

20. Huang, M.C.; Wang, T.; Chang, W.S.; Lin, J.C.; Wu, C.C.; Chen, I.C.; Peng, K.C.; Lee, S.W. Temperature Dependence on P-Cu_2O Thin Film Electrochemically Deposited onto Copper Substrate. *Appl. Surf. Sci.* **2014**, *301*, 369–377. [CrossRef]

21. Mallik, A.; Ray, B.C. Implication of Low Temperature and Sonication on Electrocrystallization Mechanism of Cu Thin Films: A Kinetics and Structural Correlation. *Mater. Res.* **2013**, *16*, 539–545. [CrossRef]

22. Mallik, A.; Ray, B.C. Evolution of Principle and Practice of Electrodeposited Thin Film: A Review on Effect of Temperature and Sonication. *Int. J. Electrochem.* **2011**, *2011*, 568023. [CrossRef]

23. Akbari, R.; Mohammadizadeh, M.R.; Khajeh Aminian, M.; Abbasnejad, M. Hydrophobic Cu_2O Surfaces Prepared by Chemical Bath Deposition Method. *Appl. Phys. A Mater. Sci. Process.* **2019**, *125*, 190. [CrossRef]

24. Dini, J.W.; Snyder, D.D. Electrodeposition of Copper. In *Modern Electroplating*; Schlesinger, M.P., Ed.; John Wiley & Sons, Inc.: Hoboken, NJ, USA, 2010; pp. 33–78. ISBN 9780470167786.

25. Zhao, W.; Fu, W.; Yang, H.; Tian, C.; Li, M.; Li, Y.; Zhang, L.; Sui, Y.; Zhou, X.; Chen, H.; et al. Electrodeposition of Cu_2O Films and Their Photoelectrochemical Properties. *CrystEngComm* **2011**, *13*, 2871–2877. [CrossRef]

26. Ding, Y.; Li, Y.; Yang, L.; Li, Z.; Xin, W.; Liu, X.; Pan, L.; Zhao, J. The Fabrication of Controlled Coral-like Cu_2O Films and Their Hydrophobic Property. *Appl. Surf. Sci.* **2013**, *266*, 395–399. [CrossRef]

27. Akbari, R.; Ramos Chagas, G.; Godeau, G.; Mohammadizadeh, M.; Guittard, F.; Darmanin, T. Intrinsically Water-Repellent Copper Oxide Surfaces; An Electro-Crystallization Approach. *Appl. Surf. Sci.* **2018**, *443*, 191–197. [CrossRef]

28. Akbari, R.; Godeau, G.; Mohammadizadeh, M.; Guittard, F.; Darmanin, T. Wetting Transition from Hydrophilic to Superhydrophobic over Dendrite Copper Leaves Grown on Steel Meshes. *J. Bionic Eng.* **2019**, *16*, 719–729. [CrossRef]

29. Akbari, R.; Godeau, G.; Mohammadizadeh, M.; Guittard, F.; Darmanin, T. The Influence of Bath Temperature on the One-Step Electrodeposition of Non-Wetting Copper Oxide Coatings. *Appl. Surf. Sci.* **2020**, *503*, 144094. [CrossRef]

30. Sau, T.K.; Rogach, A.L. *Complex-Shaped Metal Nanoparticles*; Sau, T.K., Rogach, A.L., Eds.; Wiley-VCH: Weinheim, Germany, 2012; ISBN 9783527325894.

31. Ko, W.Y.; Chen, W.H.; Der Tzeng, S.; Gwo, S.; Lin, K.J. Synthesis of Pyramidal Copper Nanoparticles on Gold Substrate. *Chem. Mater.* **2006**, *18*, 6097–6099. [CrossRef]

32. Ko, W.Y.; Chen, W.H.; Cheng, C.Y.; Lin, K.J. Highly Electrocatalytic Reduction of Nitrite Ions on a Copper Nanoparticles Thin Film. *Sens. Actuators B Chem.* **2009**, *137*, 437–441. [CrossRef]

33. Ko, W.Y.; Chen, W.H.; Cheng, C.Y.; Lin, K.J. Architectural Growth of Cu Nanoparticles through Electrodeposition. *Nanoscale Res. Lett.* **2009**, *4*, 1481–1485. [CrossRef]

34. Wang, L. *Preparation and Characterization of Properties of Electrodeposited Copper Oxide Films*; The University of Texas at Arlington: Arlington, TX, USA, 2006.

35. Giri, S.D.; Sarkar, A. Electrochemical Study of Bulk and Monolayer Copper in Alkaline Solution. *J. Electrochem. Soc.* **2016**, *163*, H252–H259. [CrossRef]

36. Kim, S.; Kim, Y.; Jung, J.; Chae, W.S. Photoassisted Electrodeposition of a Copper(I) Oxide Film. *Mater. Trans.* **2015**, *56*, 377–380. [CrossRef]

37. Free, M.; Rodchanarowan, A.; Phadke, N.; Bhide, R. Evaluation of the Effects of Additives, Pulsing, and Temperature on Morphologies of Copper Electrodeposited from Chloride Media. *ECS Trans.* **2006**, *2*, 335–343. [CrossRef]

38. Akbari, R.; Godeau, G.; Mohammadizadeh, M.R.; Guittard, F.; Darmanin, T. Fabrication of Superhydrophobic Hierarchical Surfaces by Square Pulse Electrodeposition: Copper-Based Layers on Gold/Silicon (100) Substrates. *Chempluschem* **2019**, *84*, 368–373. [CrossRef] [PubMed]

39. Chen, L.-C.; Nguyen, D.T.; Chang, Y.-W. Precise Optical Surface Profilometry Using Innovative Chromatic Differential Confocal Microscopy. *Opt. Lett.* **2016**, *41*, 5660. [CrossRef] [PubMed]

40. Vorburger, T.V.; Rhee, H.G.; Renegar, T.B.; Song, J.F.; Zheng, A. Comparison of Optical and Stylus Methods for Measurement of Surface Texture. *Int. J. Adv. Manuf. Technol.* **2007**, *33*, 110–118. [CrossRef]

41. Chand, M.; Mehta, A.; Sharma, R.; Ojha, V.N.; Chaudhary, K.P. Roughness Measurement Using Optical Profiler with Self-Reference Laser and Stylus Instrument—A Comparative Study. *Indian J. Pure Appl. Phys.* **2011**, *49*, 335–339.

42. Akbari, R.; Antonini, C. Contact Angle Measurements: From Existing Methods to an Open-Source Tool. *Adv. Colloid Interface Sci.* **2021**, *294*, 102470. [CrossRef]

43. Siegfried, M.J.; Choi, K.S. Electrochemical Crystallization of Cuprous Oxide with Systematic Shape Evolution. *Adv. Mater.* **2004**, *16*, 1743–1746. [CrossRef]

44. Siegfried, M.J.; Choi, K.-S. Directing the Architecture of Cuprous Oxide Crystals during Electrochemical Growth. *Angew. Chem.* **2005**, *117*, 3282–3287. [CrossRef]

45. Siegfried, M.J.; Choi, K.S. Elucidating the Effect of Additives on the Growth and Stability of Cu_2O Surfaces via Shape Transformation of Pre-Grown Crystals. *J. Am. Chem. Soc.* **2006**, *128*, 10356–10357. [CrossRef]

46. Siegfried, M.J.; Choi, K.S. Elucidation of an Overpotential-Limited Branching Phenomenon Observed during the Electrocrystallization of Cuprous Oxide. *Angew. Chem.-Int. Ed.* **2008**, *47*, 368–372. [CrossRef]

47. Tam, J.; Palumbo, G.; Erb, U.; Azimi, G. Robust Hydrophobic Rare Earth Oxide Composite Electrodeposits. *Adv. Mater. Interfaces* **2017**, *4*, 1700850. [CrossRef]

48. Hassebrook, A.C. *Applications of Femtosecond Laser Processed Metallic Surfaces: Leidenfrost Point and Thermal Stability of Rare Earth Oxide Coatings*; University of Nebraska-Lincoln: Lincoln, NE, USA, 2017.
49. Preston, D.J.; Miljkovic, N.; Sack, J.; Enright, R.; Queeney, J.; Wang, E.N. Effect of Hydrocarbon Adsorption on the Wettability of Rare Earth Oxide Ceramics Effect of Hydrocarbon Adsorption on the Wettability of Rare Earth Oxide Ceramics. *Appl. Phys. Lett.* **2014**, *105*, 011601. [CrossRef]
50. Boyce, J.M. Modern Technologies for Improving Cleaning and Disinfection of Environmental Surfaces in Hospitals. *Antimicrob. Resist. Infect. Control* **2016**, *5*, 10. [CrossRef] [PubMed]
51. González, C.M. Cleaning with UV Light. *Mech. Eng.* **2021**, *143*, 32–33. [CrossRef]
52. *ASTM D 4060-10*; Standard Test Method for Abrasion Resistance of Organic Coatings by the Taber. ASTM International: West Conshohocken, PA, USA, 2010. [CrossRef]
53. Zhang, Y.; Liu, J.; Ouyang, L.; Li, J.; Xie, G.; Yan, Y.; Weng, C. One-Step Preparation of Robust Superhydrophobic Foam for Oil/Water Separation by Pulse Electrodeposition. *Langmuir* **2021**, *37*, 7043–7054. [CrossRef]